Vol. 4, No. 1 (2023); 1 – 17

Journal of Earth Sciences and Technology

http://www.htpub.org/Journal-Of-Earth-Sciences-And-Technology/

Feasibility Study of CO_2 Sequestration on Depleted Carbonate Reservoir Using Rockphysics and Seismic Forward Modeling, Central Luconia Sarawak Case Study

Angel An Qi Lee[a], Maman Hermana[a]*

[a]*Department of Geoscience, Universiti Teknologi PETRONAS, 32610 Seri Iskandar, Perak, Malaysia*

Article Information

Article History
Received: 14/12/2022
Accepted: 08/02/2023
Available online: 02/03/2023

Keywords
CO_2 sequestration
Feasibility Study
Rock Physics
Depleted Carbonate Reservoir

Abstract

Carbon dioxide, CO_2 sequestration is a feasible solution to reduce the amount of CO_2 in the Earth's atmosphere. However, constant monitoring of the CO_2 effect after the injection is important to ensure safe and prolonged storage of the CO2 in the geological site. This study is about the feasibility study of CO_2 sequestration in a depleted carbonate reservoir in Central Luconia, Sarawak, Malaysia using rock physics and seismic forward modeling. Two well log datasets from Central Luconia are used in this study. Hampson-Russell Software and Microsoft Excel are utilized to obtain the results. In this paper, Gassmann Fluid Substitution Model is used to study the elastic properties change in the depleted carbonate reservoir due to the injection of CO_2. 1D seismic forward modeling is generated from the P-wave velocity, S-wave velocity and density acquired for the different case scenarios to study the effect of CO_2 towards the seismic response. Post-Stack and Pre-Stack seismic attributes are generated to determine the most sensitive seismic attributes for identifying CO_2 injection effects through qualitative and quantitative analysis. Elastic properties such as P-Impedance, Vp/Vs ratio, Lambda-Rho, Mu-Rho, SQp and SQs are calculated. A number of elastic properties cross plots are generated to select the best elastic properties for CO_2 monitoring. Based on the findings, the feasibility study of CO_2 sequestration in Central Luconia depleted carbonate reservoir using rock physics and seismic forward modeling is proven to be viable.

1.Introduction

Carbon dioxide, CO_2 sequestration is the storage of carbon dioxide in geological structures to reduce the amount of CO_2 in the Earth's atmosphere. To trap the CO2, CO2 generated from either natural point sources

* Corresponding author
E-mail address: maman.hermana@utp.edu.my

or human activities is captured and injected into layers with porosity surrounded by non-porous layers (Hovorka, 2008; Vera & Lawton, 2010). Increase of the CO_2 in the atmosphere had been a concerning problem as CO_2 is one of the greenhouse gases which cause global warming. For years, various feasibility studies had been carried out to monitor and ensure the safe injection of CO2 and permanent storage of the gas in suitable geological sites.

To ensure the injected CO_2 migrates into the storage site and there is no leakage, constant monitoring of the CO_2 during and after injection is essential (Raza, Gholami, Rezaee, Rasouli & Rabiei, 2019). Leakage of the CO_2 due to the CO_2 sequestration will lead to an increase in the CO_2 concentration in the subsurface layer which will eventually pollute the groundwater as well as causing deadly effects on the subsoil animals and plants. CO_2 fluxes due to the stable atmospheric conditions will cause the concentrations of CO_2 in the air to rise and this will affect the living beings on Earth. Hence, it is critical to ensure that no leakage happens during the process of CO_2 sequestration.

In recent years, various methods had been introduced for the monitoring of the geological site of CO_2 sequestration. For instance, seismic monitoring, geoelectrical methods, temperature logs, gravity methods, remote sensing, geochemical sampling, tracers, soil gas and microbiology (Leung, Caramanna & Maroto-Valer, 2014). However, there are still limitations to these studies, hence more studies and research are required to improve the methods to monitor the CO_2 plume migration.

Seismic method is used to monitor the evolution of the CO_2 during and after the injection of CO_2. For example, a three-dimensional image of the subsurface structures together with the dimension of the injected plume of CO_2 is generated by the 3D seismic. The evolution through the time of CO_2 plume is tracked by using time lapse or 4D monitoring (Leung et al.,2014). There had been studies done on the application of seismic method to monitor the CO_2 plume migration in clastic reservoirs, particularly in a sandstone aquifer by Vera & Lawton (2010). As opposed to clastic reservoirs, carbonate reservoirs are still poorly understood (Moghanloo, 2017). There are more challenges to implement CO_2 sequestration in a carbonate reservoir. For instance, mineralization will happen due to the dissolution of CO_2 into the water, therefore more research is needed before acquiring carbonate reservoir as a suitable CO_2 sequestration site. (Moghanloo, 2017).

In this study, the Gassmann Fluid Substitution model will be used for the estimation of the effects and changes of the elastic properties as the CO_2 is injected into a depleted carbonate reservoir in Central Luconia. The seismic response generated from the different saturation of injected CO_2 will be acquired through seismic forward modeling. Various seismic attributes will be generated, and the most sensitive seismic attributes will be selected to identify the CO_2 injection effects. The best elastic properties for the monitoring of CO_2 injection will be determined through analyzation of elastic properties cross plot.

2. Dataset and Methodology

2.1 Dataset

Well logs dataset from Central Luconia, Sarawak, Malaysia is provided to conduct the study. In this study, two well logs, Well A and Well B are used. Well A has all the logs which are Gamma Ray, Density, Porosity, Permeability, Water Saturation, P-wave velocity, and S-wave velocity logs, whereas in Well B, S-wave velocity log is not available.

2.2 Methodology

The methods used for the feasibility study of the CO_2 sequestration on depleted carbonate reservoir is shown in figure 3.1.

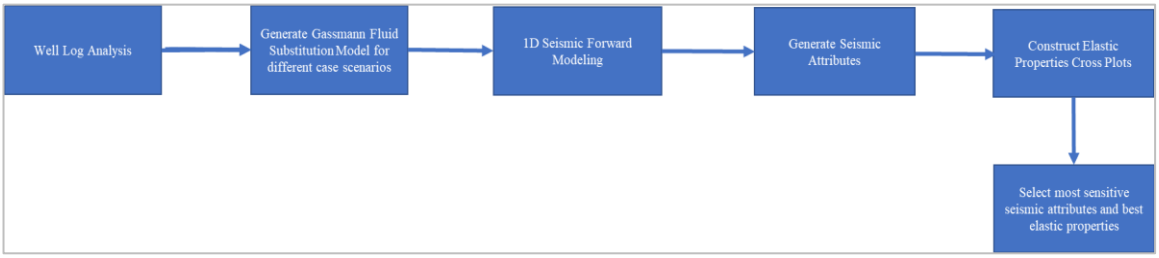

Fig. 1. Summary of project workflow.

The reservoir interval for both Well A and Well B is determined based on the petrophysical properties. In Well B, prediction of the S-wave velocity log is conducted using Greenberg-Castagna method inside the reservoir and Castagna method on the outside of the reservoir. The reliability of these methods for the prediction of S-wave velocity in Well B is justified based on the accuracy of the prediction of S-wave velocity in Well A. The predicted S-wave velocity is compared with the actual S-wave velocity in Well A and cross plot of the S-wave velocity comparison is generated to identify the R value and R-square value to determine the accuracy of the methods. The accuracy of the predicted S-wave velocity is also justified through the comparison of the P-wave velocity logs and the S-wave velocity logs of both Well A and Well B to determine if the S-wave velocity logs follow the P-wave velocity logs trend.

Gassmann Fluid Substitution Model is generated in the Hampson-Russell Software (HRS) to analyse the P-wave velocity, S-wave velocity and density values change in the carbonate reservoir due to CO_2 injection. In this study, five case scenarios are conducted which are 100% Brine, 100% Gas, 100% CO_2, 80% CO_2+ 20% Brine and 50% CO_2+ 50% Brine. The property of the CO_2 is specified by calculating the CO_2 using the FLAG 2014 method. According to Oldenburg, Pruess and Benson (2000), the range of temperature in depleted natural gas reservoir is from 27 to 120 degree Celsius and the range of pressure is from 20 to 50 bar. The geothermal gradient of the first 3 to 5 km of the Earth is approximately 25 degrees Celsius per km (DiPietro,2013). Henceforward, in this study, the temperature of the Carbonate reservoir interval is specified at 80 degrees Celsius, and the pressure is specified at 35 bar.

1D seismic forward modeling is generated to study the effect of CO_2 injection on the seismic response. Synthetic seismogram for each case scenarios which are 100% Brine, 100% Gas, 100% CO_2, 80% CO_2 +20%Brine and 50% CO_2 +50% Brine is generated. In this process, pre-stack synthetics is generated using Aki-Richards algorithm. The number of angles is specified at 10 with 0 degree as the near angle and 30 degrees as the far angle. Ricker wavelet of 90Hz is used to create the synthetic seismogram. The frequency of Ricker wavelet is specified at 90Hz to increase the seismic resolution of the produced synthetic seismogram.

The most sensitive seismic attribute is selected to identify the effects of CO_2 injection. Two types of seismic attributes which are the post stack attributes and the pre stack attributes are generated. The amplitude envelope, amplitude weighted frequency and instantaneous frequency which are the post stack attribute and the Amplitude Versus Offset (AVO) attribute which is the pre-stack attribute are the seismic attributes generated in this study. In this section, only two case scenarios are focused on which are the 100% Brine and the 100% CO_2. In quantitative analysis of the seismic attributes, the contrast between the two case scenarios which are 100% Brine, and 100% CO_2 are calculated quantitatively and tabulated in a table to determine the most sensitive seismic attributes for CO_2 injection effects. To perform quantitative analysis, the trace amplitude value of each seismic attributes at the top reservoir for both cases are used to calculate the delta to indicate the sensitivity of the seismic attribute for identifying CO_2injection effects. The larger the value of delta, the more sensitive is the seismic attributes for identification of CO_2 injection effects. The delta (δ) is calculated using the formula stated in equation (1).

$$\delta = \left| \frac{A_{100\%Brine} - A_{100\%CO2}}{A_{100\%Brine}} \right| \quad (1)$$

where A is the different seismic attributes used.

The calculated delta is tabulated in a table using Microsoft Excel to compare the result for the post-stack and pre-stack seismic attributes to select the most sensitive post-stack and pre-stack seismic attributes for identifying CO_2 injection effects. To identify the best elastic properties for CO_2 injection monitoring, cross plots of elastic properties are generated in this study. A total of three elastic cross plots are generated, which are P-Impedance vs Vp/Vs ratio, Lambda-Rho vs Mu-Rho and SQs vs SQp cross plots. Before constructing the cross plots, the elastic properties such as P-Impedance, Vp/Vs ratio, S-Impedance, Lambda-Rho, Mu-Rho, SQs and SQp are calculated for the two case scenarios which are 100% Brine and 100% CO_2 using Hampson Russell Software. Subsequently, the cross plots are generated and the best elastic properties to monitor CO_2 injection is determined by analysing the cross plots.

3. Results and Discussions

3.1 Identification of Carbonate Reservoir Interval

The carbonate reservoir interval is determined for Well A and Well B. Generally, carbonate reservoir has low gamma ray readings, low density, and water saturation readings, as well as high porosity and permeability readings. The identified carbonate reservoir intervals in Well A and Well B are as shown in Figure 2 and Figure 3 respectively.

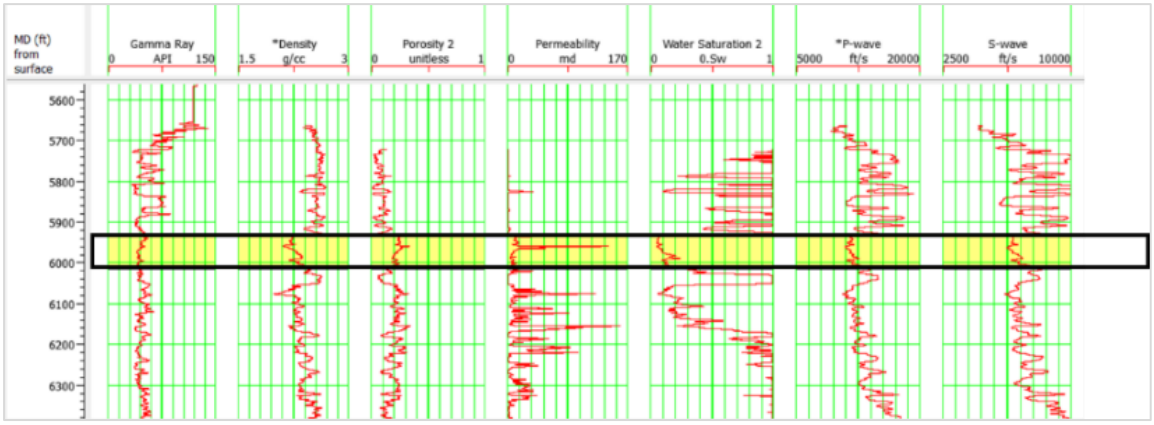

Fig. 2. Well log view of Well A. The reservoir interval is as shown in the black box.

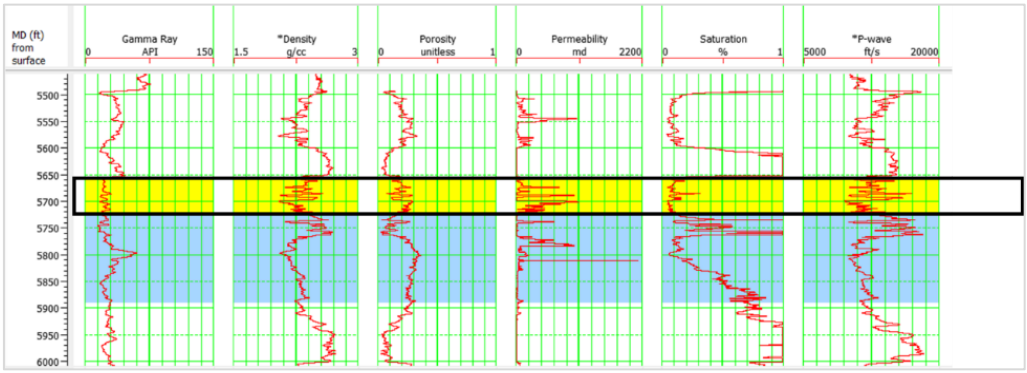

Fig. 3. Well log view of Well B. The reservoir interval is as shown in the black box.

The carbonate reservoir interval in Well A is determined at an interval of 5933ft MD to 6015ft MD, whereas in Well B, the reservoir interval is identified at an interval of 5658ft MD to 5723ft MD.

The carbonate reservoir interval is determined by first analysing the gamma ray logs which indicates the lithology of the specific interval of wells. Low gamma ray values from the interval represents carbonate lithology. Next, referring to the density and water saturation logs, low readings will indicate potential hydrocarbon accumulation. High readings of porosity and permeability logs are also indication of potential reservoir at the specific interval of wells.

3.2 Shear Wave Velocity Prediction

Due to the missing shear wave or S-wave velocity in Well B, prediction of S-wave velocity is required before proceeding with the Gassmann Fluid Substitution Model. In Well A, S-wave velocity is available from the provided well log dataset. Hence, prediction of S-wave velocity is carried out in Well A to investigate the accuracy of the empirical methods before proceeding with the prediction of S-wave velocity in Well B. Greenberg-Castagna Method is applied for the prediction of S-wave velocity inside the reservoir whereas Castagna Method is applied for the prediction of S-wave velocity outside the reservoir interval. Figure 4 shows the prediction of S-wave velocity using the Greenberg-Castagna and Castagna method in Well A.

In figure 4, the prediction of S-wave using Greenberg-Castagna Method inside of the reservoir interval and Castagna Method outside of the reservoir interval shows high accuracy of prediction. The comparison between the predicted S-wave and the original S-wave velocity from the well log dataset in well view is shown on the left side of the figure. The predicted S-wave velocity matches almost exactly with the original S-wave velocity provided from the well log dataset. On the right side of Figure 4.3, the cross plot shows high R-value of 0.971482 and a R-square value of 0.9438, indicating high accuracy of prediction using the proposed method.

Based on the result in Well A, the S-wave velocity in Well B is predicted using the Greenberg-Castagna and Castagna Method. Figure 5 shows the prediction of the S-wave velocity in Well B using Greenberg-Castagna method inside of the reservoir and Castagna Method outside of the reservoir. Another justification of the accuracy of the S-wave velocity prediction in Well B is made based on the comparison of the P-wave velocity with the S-wave velocity in both wells. Figure 6 shows the comparison of both P-wave velocity and S-wave velocity in Well A and Well B.

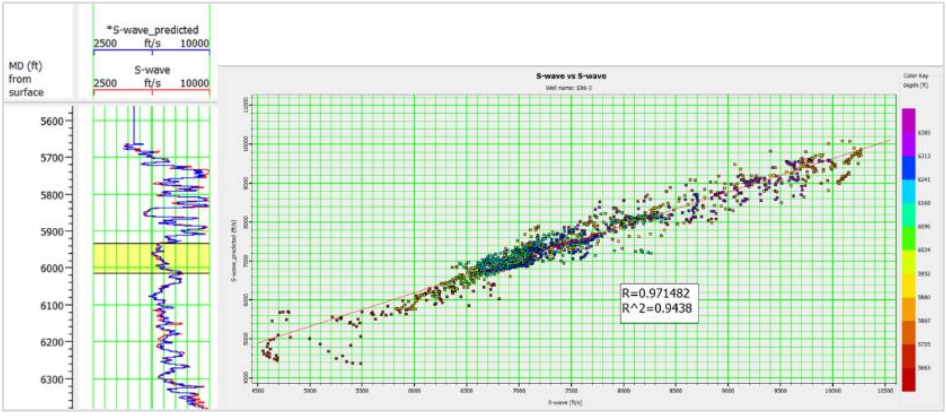

Fig. 4. Prediction of S-wave in Well A.

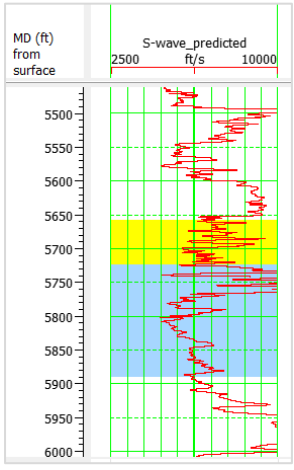

Fig. 5. Predicted S-wave velocity log in Well B.

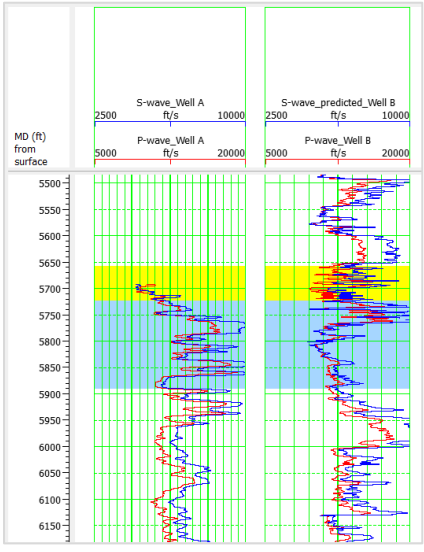

Fig. 6. Comparison of P-wave velocity and S-wave velocity in Well A and Well B.

By comparing the P-wave velocity and S-wave velocity in Well A, the S-wave velocity follows the trend of the P-wave velocity. For Well B, the predicted S-wave velocity follows the trend of the P-wave velocity as well. Therefore, the predicted S-wave velocity in Well B using the Greenberg-Castagna method inside the reservoir and the Castagna method outside the reservoir is proven to have high accuracy and both these models are suitable to predict the missing S-wave in Well B.

3.3 Gassmann Fluid Substitution

There are a total of five case scenarios generated as the outcome for each well using the Gassmann Fluid Substitution Model. The five case scenarios are 100% Brine, 100% Gas, 100% CO_2, 80% CO_2 + 20% Brine and 50% CO_2 + 50% Brine.For each case scenarios of both Well A and Well B, the elastic properties which include the density values, P-wave velocities and S-wave velocities logs generated from the Gassmann Fluid Substitution Model are analyzed. Figure 7 shows the comparison of the density logs of different case scenarios in reservoir interval in Well A and Well B.

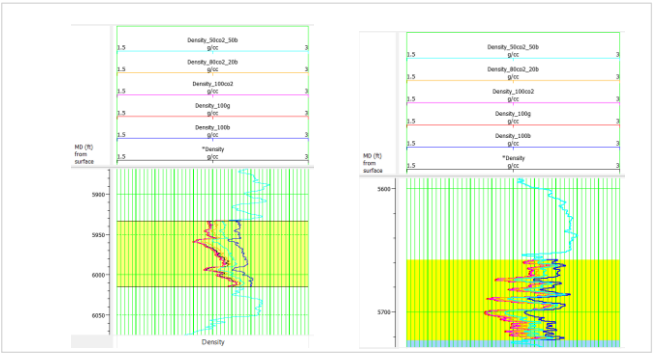

Fig. 7. Comparison of density logs of different case scenarios in reservoir interval in Well A (left) and Well B (right).

In general, the density logs with 100% brine (blue line) shows the highest density values, followed by the density logs with 50% CO_2+ 50% Brine (light blue line), the density logs with 80% CO_2 + 20% Brine (orange line), density logs with 100% CO_2 (purple line) and lastly density logs with 100% Gas (red line) with the lowest density values. There is a high contrast in density values when reservoir with 100% brine is replaced with 100% CO_2. There is only slight contrast when comparing the density values of reservoir with 100% gas and 100% CO_2, but the differences are still noticeable. Reservoir with high brine saturation shows high density reading, followed by reservoir with high CO_2 and lastly reservoir with high hydrocarbon gas. Using the Gassmann Fluid Substitution model, the density values change in depleted carbonate reservoir because of CO_2 injection can be estimated as there is high contrast between the density values of 100% Brine and 100% CO_2 case scenarios. Figure 8 shows the comparison of the P-wave velocity logs of different case scenarios in reservoir interval in Well A and Well B.

The P-wave velocities generally is the highest in 100% Brine (blue line) case scenarios, followed by 100% Gas (red line) ,100% CO_2 (purple line), 80% CO_2 +20% Brine (orange line) and lastly the 50% CO_2+50% Brine (light blue line). In high brine saturation reservoir, the P-wave velocity is high due to the high bulk modulus and high-density values. There is a high contrast in the P-wave velocity logs in 100% Brine and 100% CO_2 case scenarios. The P-wave velocity values is lower in 100% CO_2 because the bulk modulus and density of CO_2 is lower compared to brine. There is smaller contrast in the P-wave velocity logs in 100% CO_2 and 100% Gas scenarios, but the differences are still noticeable. For the case scenarios with mix fluids of 80% CO_2+20% Brine and 50% CO_2+50% Brine, the P-wave velocities are lower compared because of decreasing in bulk modulus is more prominent in these case scenarios compared to the decrease of density. Application of Gassmann Fluid Substitution model in this study helps to evaluate

the changes in the P-wave velocities when there is injection of CO_2 in the depleted carbonate reservoir especially there is high contrast of P-wave velocities between the 100% Brine and 100% CO_2 case scenarios.

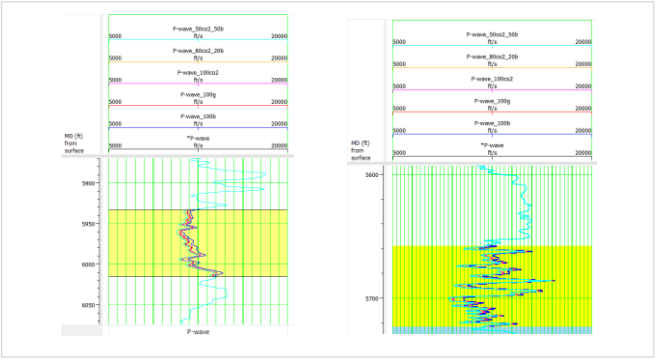

Fig. 8. Comparison of P-wave velocity logs of different case scenarios in reservoir interval in Well A (left) and Well B (right).

Figure 9 shows the comparison of the P-wave velocity logs of different case scenarios in reservoir interval in Well A and Well B.

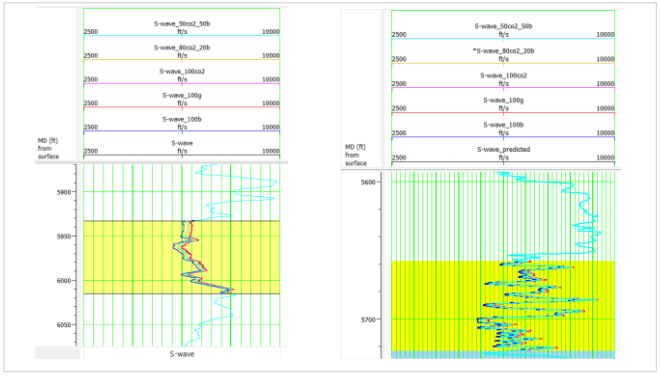

Fig. 9. Comparison of S-wave velocity logs of different case scenarios in reservoir interval in Well A (left) and Well B (right).

For S-wave velocities, there is not much significant changes compared to elastic properties such as density and P-wave velocities. The changes in the S-wave velocities are not affected by the shear modulus as the S-waves do not travel through fluids, hence S-wave velocities depends solely on the changes in bulk modulus. Therefore, in general, S-wave velocities is higher in reservoir with high gas saturation. In this thesis, the S-wave velocity is the highest for 100%Gas (red line), followed by 100% CO_2 (purple line), 80% CO_2+20% Brine (orange line), 50% CO_2+50% Brine (light blue line) and lastly 100% Brine (blue line).

The elastic properties changes in the carbonate reservoir due to CO_2injection which include the density, P-wave velocities and S-wave velocities can be estimated and analysed using the Gassmann Fluid Substitution Model. Replacement of brine with CO_2 in the depleted carbonate reservoir show significant changes in the elastic properties especially the density and P-wave velocities using the Gassmann Fluid Substitution Model.

3.4 Seismic Forward Modeling

Seismic Forward Modeling is generated to produce seismic response for each of the case scenarios which are 100%Brine, 100%Gas, 100% CO_2, 80% CO_2+20%Brine and 50% CO_2+50% Brine for both Well A and Well B. Figure 10 shows the synthetic seismogram produced for 100% Brine, 100% Gas and 100% CO_2 case scenarios in Well A and Well B. The top and bottom reservoir are shown with the red lines in the figure.

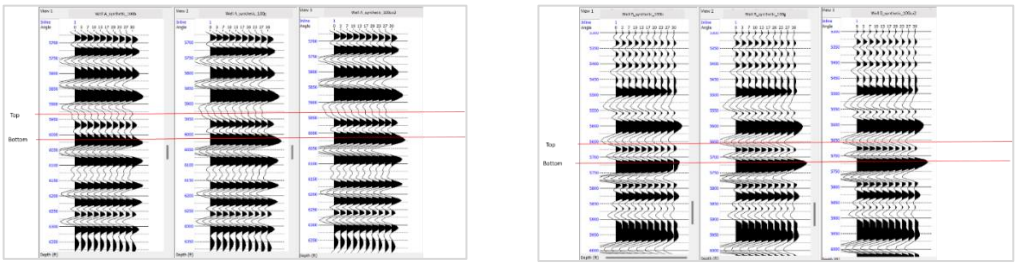

Fig. 10. Synthetic Seismogram of 100%Brine, 100%Gas and 100% CO2 in Well A (left) and Well B (right).

In general, the results show that the amplitude of 100% brine increases with offset, but the 100% CO_2 decreases with offset. There is no major variation between the 100% Gas and 100% CO_2 synthetic seismogram. However, the differences between the 100% Brine and 100% CO_2 synthetic seismogram are significant to show there is differences in the seismic response when CO_2 is injected into a depleted carbonate reservoir with brine.

Figure 11 shows the synthetic seismogram produced for 100% CO_2, 80% CO_2+20% Brine and 50% CO_2 +50% Brine case scenarios in Well A and Well B. The top and bottom reservoir are shown with the red lines in the figure.

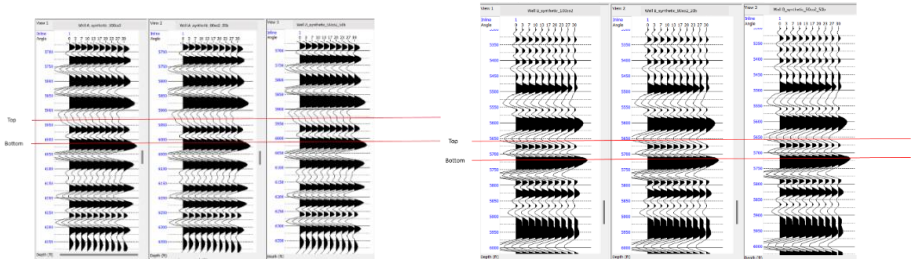

Fig. 11. Synthetic Seismogram of 100% CO2 ,80% CO2+20%Brine and 50% CO2+50%Brine in Well A (left) and Well B (right).

There is no major variation in the amplitudes of the seismic traces when the saturation of CO_2 changes from 100% to 80% and to 50%. Overall, there is significant differences in the seismic response between the 100% Brine and 100% CO_2 case scenarios. The 100% brine amplitude increases with increasing offset whereas the 100% CO_2 decreases with increasing offset. There is no major difference in the synthetic traces of the 100% CO_2 when compared to 100% Gas and when the CO_2 saturation changes from 100% to 80% and to 50%. Nevertheless, the seismic response will display significant differences when the CO_2 is injected into depleted carbonate reservoir filled with brine.

3.5 Seismic Attributes

In this study, post-stack and pre-stack seismic attributes are generated to identify the best seismic attributes for the CO_2 injection effects. The post-stack attributes generated are the amplitude envelope,

amplitude weighted frequency and instantaneous frequency attributes, whereas for the pre-stack attributes, the amplitude versus offset (AVO) attribute is generated. The seismic attributes are generated for the 100%Brine and 100% CO_2 case scenarios for both Well A and Well B. Qualitative and quantitative analysis are carried out for the seismic attributes to determine the most sensitive seismic attributes.

3.5.1 Post-Stack Seismic Attribute

The first post-stack seismic attributes generated is the amplitude envelope. Figure 12 shows the result of the seismic attribute in both Well A and Well B. The top and bottom reservoir are shown with the red lines in the figure.

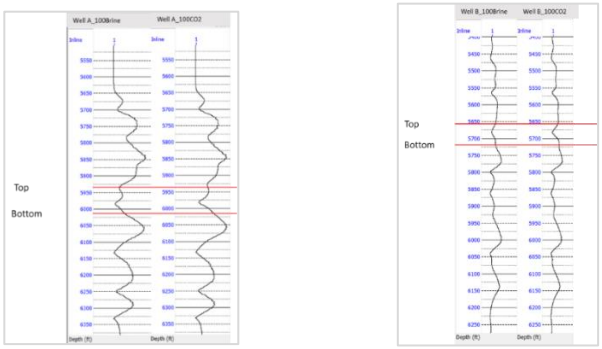

Fig. 12. Amplitude envelope generated for 100% Brine and 100% CO2 in Well A (left) and Well B (right).

The trace amplitude values of the amplitude envelope for 100% CO_2 are shown to be greater than the amplitude envelope for 100% Brine at the top reservoir in both wells. Figure 13 shows the amplitude weighted frequency generated in both Well A and Well B. The top and bottom reservoir are shown with the red lines in the figure.

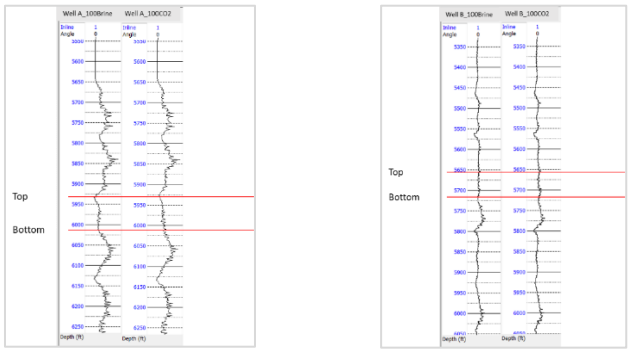

Fig. 13. Amplitude weighted frequency generated for 100% Brine and 100% CO2 in Well A (left) and Well B (right).

The trace amplitude values of the amplitude weighted frequency are shown to have higher amplitude values in 100% CO_2 compared to 100% Brine at the top reservoir compared in both wells although the difference is not that noticeable.

Figure 14 shows the instantaneous frequency generated in both Well A and Well B. The top and bottom reservoir are shown with the red lines in the figure.

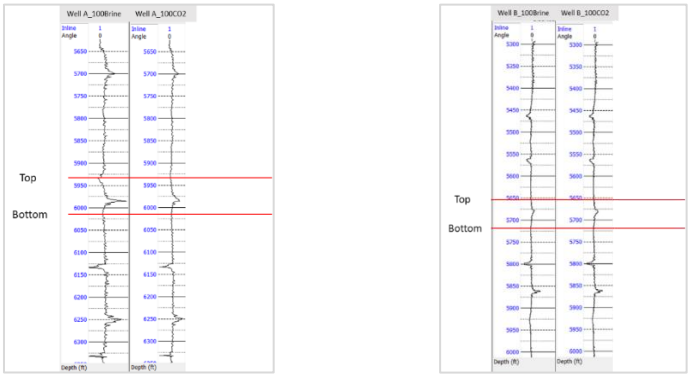

Fig. 14. Instantaneous frequency generated for 100% Brine and 100% CO2 in Well A (left) and Well B (right).

The instantaneous frequency amplitude values at the top reservoir are greater in the 100% CO_2 compared to 100% Brine in Well A. However, in Well B, the instantaneous frequency at the top reservoir in 100% Brine has greater amplitude values than 100% CO2. However, the contrast between the two cases at the top reservoir are not highly distinguishable through comparison of the seismic traces, therefore quantitative analysis will be needed.

3.5.2 Pre-Stack Seismic Attributes

The pre-stack seismic attributes generated is the amplitude versus offset (AVO) attribute. Intercept (a) and Gradient (b) are the attributes of AVO generated in this thesis. Figure 15 shows the Intercept (a) of AVO attribute generated in both Well A and Well B. The top and bottom reservoir are shown with the red lines in the figure.

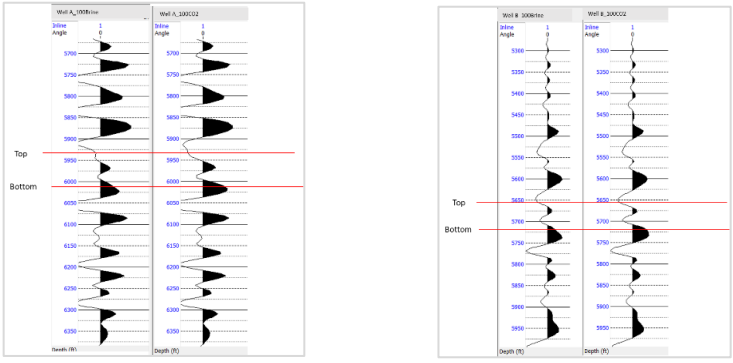

Fig. 15. Intercept (a) attribute generated for 100% Brine and 100% CO2 in Well A (left) and Well B (right).

The amplitude of the seismic traces at the top reservoir of 100% Brine can be seen to have greater values than 100% CO_2 in both wells. Figure 16 shows the gradient (b) of AVO attribute generated in both Well A and Well B. The top and bottom reservoir are shown with the red lines in the figure.

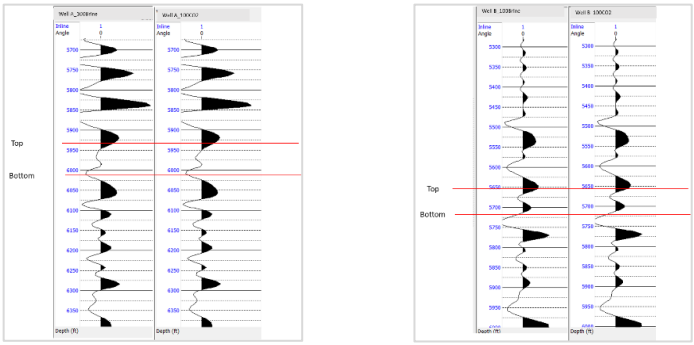

Fig. 16. Gradient (b) attribute generated for 100% Brine and 100% CO2 in Well A (left) and Well B (right).

There are no distinct and noticeable differences between the amplitude values at top reservoir of 100% Brine and 100% CO_2 case scenarios in the gradient (b) attribute. Cross plots of AVO and further quantitative analysis will be needed to determine the sensitivity of the seismic attributes due to the contrast between the top reservoir of the 100% brine and 100% CO_2 is not distinct enough through qualitative analysis.

3.5.3 Quantitative Analysis of the Seismic Attributes

Before proceeding to quantitatively calculate the contrast between the two case scenarios (e.g., 100% Brine and 100% CO_2), AVO cross plot are calculated using the trace amplitude values of the each AVO attribute which is Intercept (a) and Gradient (b) at the top reservoir only. Figure 17 shows the AVO cross plot of Intercept (a) vs Gradient (b) for Well A and Well B.

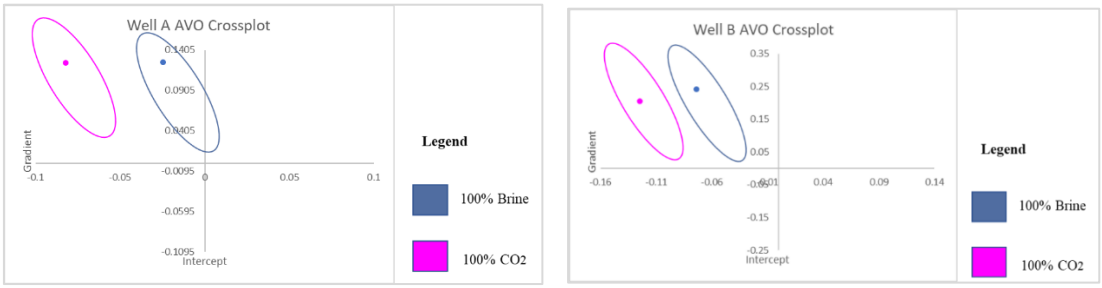

Fig. 17. AVO Intercept (a) vs Gradient (b) cross plot for Well A (left) and Well B (right).

Based on the AVO cross plots of both Well A and Well B, the top reservoir is categorized to be Class IV response for both 100% Brine and 100% CO_2. However, there are fair separations between the 100% brine and 100% CO_2 in the cross plots. The 100% CO_2 has more negative intercept (a) attribute values as compared to 100% Brine. The gradient (b) attribute of both cases is almost the same and no obvious differences are displayed.

To further analyse the sensitivity of the seismic attributes generated for both cases, quantitative calculation is done by calculating the delta of the seismic attributes of 100% Brine and 100% CO_2. Table 1 and 2 shows the delta values for the post-stack and pre-stack seismic attributes generated in Well A and Well B respectively. The seismic attributes with the highest delta values will be most sensitive for CO_2 identification.

Table 1. Delta calculated for post-stack and pre-stack seismic attributes for Well A.

Type	Seismic Attributes	100b	100co2	Delta
Post-stack	Amplitude Envelope	0.043625	0.089184	1.044328
	Amplitude Weighted Frequency	-0.19368	0.647026	4.340627
	Instantaneous Frequency	-4.47401	7.25884	2.622446
Pre-stack	AVO Intercept (a)	-0.02472	-0.08203	2.318047
	AVO Gradient (b)	0.124973	0.123925	0.008386

Table 2. Delta calculated for post-stack and pre-stack seismic attributes for Well B.

Type	Seismic Attributes	100b	100co2	Delta
Post-stack	Amplitude Envelope	0.110687	0.149556	0.351161
	Amplitude Weighted Frequency	1.57659	1.95184	0.238014
	Instantaneous Frequency	14.2437	13.0509	0.083742
Pre-stack	AVO Intercept (a)	-0.07347	-0.12459	0.695775
	AVO Gradient (b)	0.240212	0.20567	0.143798

In table 1, the post-stack seismic attribute with the highest delta value is the amplitude weighted frequency. The delta value is 4.34 Hz. This indicates that the amplitude weighted frequency seismic attribute is the most sensitive post-stack attribute in Well A to identify the CO_2 injection effects. As for the pre-stack attribute, the most sensitive attribute is the AVO intercept (a) attribute. The delta value is 2.318. In Well A, the most sensitive post-stack seismic attribute is amplitude weighted frequency, and the most sensitive pre-stack seismic attribute is the AVO intercept (a) attribute.

In table 2, the post-stack seismic attribute with the highest delta value is the amplitude envelope attribute with the delta value of 0.351. This indicates that the amplitude envelope is the most sensitive post-stack attribute in Well B to identify the CO_2 injection effects. As for the pre-stack attribute, the most sensitive attribute is the AVO intercept (a) attribute as well. The delta value is 0.696. In Well B, the most sensitive post-stack seismic attribute is the amplitude envelope attribute, and the most sensitive pre-stack seismic attribute is the AVO intercept (a) attribute.

Overall, the most sensitive post-stack attribute is the amplitude weighted frequency and the amplitude envelope, whereas for the most sensitive pre-stack attribute is the AVO intercept (a).

3.6 Elastic Properties Cross Plots

To select the best elastic properties for CO_2 injection monitoring, several other elastic properties are calculated, and cross plots of the elastic properties are generated for the 100% Brine and 100% CO_2 case scenarios. The cross plots generated include the P-Impedance vs Vp/Vs Ratio, Lambda-Rho vs Mu-Rho and SQs vs SQp. Figure 18 shows the cross plot of P-Impedance vs Vp/Vs Ratio for Well A and Well B.

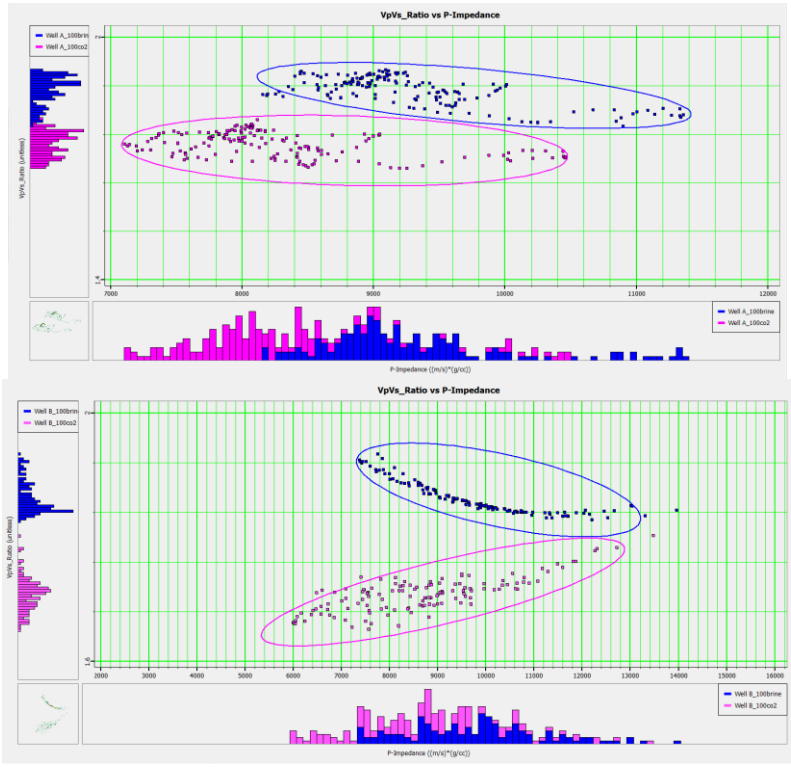

Fig. 18. Cross plot of P-Impedance vs Vp/Vs Ratio in Well A (above) and Well B (below).

The P-Impedance vs Vp/Vs ratio cross plot is used to distinguish the lithology types of the reservoir. Generally, the hydrocarbon gas has lower values of P-Impedance and Vp/Vs ratio compared to brine. From both cross plots, the 100%brine case scenarios P-Impedance and Vp/Vs ratio have higher values compared to the 100% CO_2. Both cross plots show noticeable separations between the two cases, but there are overlapping of the values especially in the P-Impedance values based on the histograms on both x and y axis. Figure 19 shows the cross plot of Lambda-Rho vs Mu-Rho for Well A and Well B.

The Lambda-Rho vs Mu-Rho (LMR) cross plot is another cross plot frequently used to discriminate the lithology types and pore fluids of the reservoir. Generally, high Mu-Rho and low Lambda-Rho values indicate gas or oil saturations whereas low Mu-Rho and high Lambda-Rho values will indicate brine saturations. From the cross-plots, the 100% brine case scenarios have low Mu-Rho and high Lambda-Rho values and the 100% CO_2 have high Mu-Rho and low Lambda-Rho values. The separation of both case scenarios, which are 100% brine, and 100% CO_2 in the cross plots are fairly separated as well, but there is overlapping of values in both Lambda-Rho and Mu-Rho values based on the histogram on both x and y axis. Figure 20 shows the cross plot of SQs vs SQp for Well A and Well B.

Based on the SQs vs SQp cross plots, these cross plots show distinct separation between the two case scenarios, which are 100%Brine and 100% CO_2. The SQs is sensitive to the separation of reservoir fluid types whereas the SQp is sensitive to discriminate the lithology of the reservoir. High SQs values indicates hydrocarbon bearing sand, while low SQs values indicate brine sand. From the results, the 100% Brine SQs is mainly scattered on the left side of the cross plot and the 100% CO_2 SQs is scattered on the right side of the cross plot. As for the SQp values, high SQp values indicate shale lithology whereas low values indicate sand. The SQp value of the 100% Brine and 100% CO_2 is generally low from cross plots of both wells. From the cross plots, the distinct separation between the 100% Brine and 100% CO_2 are shown on the

histogram of both axes as well. Hence, the SQs vs SQp cross plot is excellent for the monitoring of CO_2 injection.

In short, from the cross plots generated which are P-Impedance vs Vp/Vs ratio, Lambda-Rho vs Mu-Rho and SQs vs SQp cross plots, the most robust cross plots which display most distinct separation between the 100% brine and 100% CO_2 is the SQs vs SQp cross plot. Therefore, the SQs and SQp elastic properties are the best elastic properties to be used for CO_2 injection monitoring in depleted carbonate reservoir.

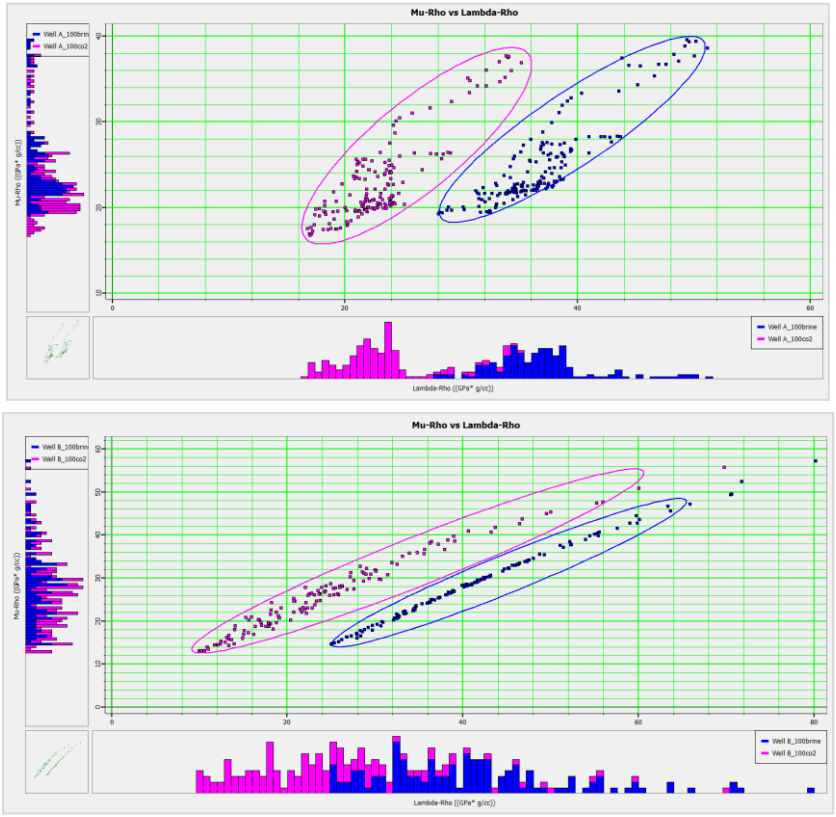

Fig. 19. Cross plot of Lambda-Rho vs Mu-Rho in Well A (above) and Well B (below).

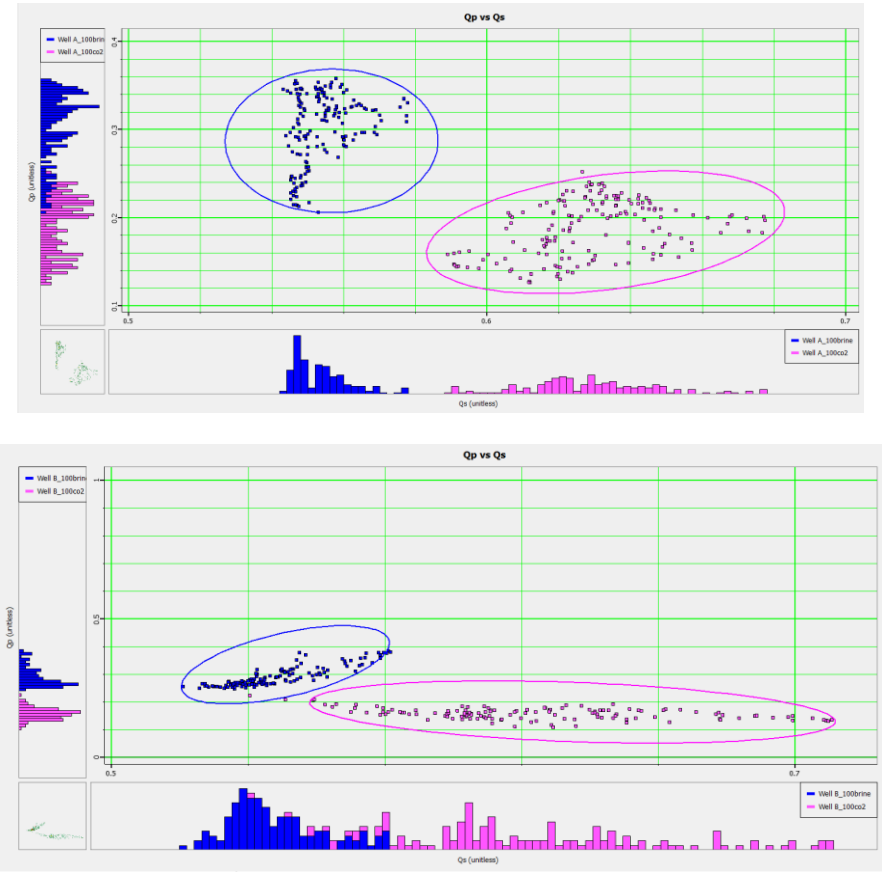

Fig. 20. Cross plot of SQs vs SQp in Well A(above) and Well B (below).

4. Conclusion

In conclusion, the feasibility study of the CO_2 sequestration in depleted carbonate reservoir using rock physics and seismic forward modelling is a viable and significant method to identify the effect of CO_2 injection. Prediction of the S-wave velocity log in one of the wells using Greenberg-Castagna and Castagna method are proven to have high accuracy as well. The Gassmann Fluid Substitution Model is successfully applied to study how changes of the fluid saturation affect the density, P-wave velocity, and S-wave velocity. Seismic forward modeling is generated for all the case scenarios to study the seismic response of different CO_2 injection scenario. The significant contrast in the synthetic seismogram of the 100% brine and 100% CO_2 indicates that when a brine saturated depleted reservoir is injected with CO_2, the effect of the injection can be observed in the seismic response. For seismic attributes, post stack attributes which are the amplitude envelope and amplitude weighted frequency are most sensitive, whereas for pre-stack attribute AVO specifically the intercept (a) attribute show high sensitivity to detect the effects of CO_2 injection through qualitative and quantitative analysis of each seismic attributes towards the 100% Brine and 100% CO_2 case scenarios. The best elastic properties for CO_2 injection monitoring are selected based on the results of the elastic properties cross plots. The SQs vs SQp cross plots display the most distinct separation, indicating that the SQs and SQp are the best elastic properties to monitor the CO_2 injection. Lambda-Rho vs Mu-Rho and P-Impedance vs Vp/Vs Ratio cross plots show only fair separation as compared to the SQs vs SQp cross plot. In general, the feasibility study of the CO_2 sequestration using rock

physics and seismic forward modeling in the Central Luconia depleted carbonate reservoir is proven to be viable and the all the objectives have been achieved.

References

Boruah, N. (2010). Rock physics template (RPT) analysis of well logs for lithology and fluid classification. In 8th International Conference Exposition on Petroleum Geophysics. Hyderahad: SPG (pp. 1-8).

Chopra, S., & Marfurt, K. J. (2008). Emerging and future trends in seismic attributes. *The Leading Edge*, 27(3), 298-318.

Close, D., Taylor, R., & Nixon, S. (2015). Rock physics and quantitative interpretation using lambda-mu-rho in the Shipwreck Trough, Otway Basin. ASEG Extended Abstracts, 2015(1), 1-4.

Gutierrez, M., Katsuki, D., & Almrabat, A. (2012). Effects of CO 2 injection on the seismic velocity of sandstone saturated with saline water. *International Journal of Geosciences*, 3(05), 908.

Haga, L. (2016). Seismic attribute analysis and CO2 monitoring within the Mississippian reservoir, Wellington field, Sumner County, Kansas (Doctoral dissertation, University of Kansas).

Hamdan, N. H., & Jamaludin, S. F. (2018). Reservoir characteristics of carbonates build-ups in southern Central Luconia Province: A study based on different scales. *Bulletin of the Geological Society of Malaysia*, 66.

Hermana, M., Ghosh, D. P., & Sum, C. W. (2016, March). Optimizing the lithology and pore fluid separation using attenuation attributes. In Offshore Technology Conference Asia. OnePetro.

Leung, D. Y. C., Caramanna, G., & Maroto-Valer, M. M. (2014). An overview of current status of carbon dioxide capture and storage technologies. *Renewable & Sustainable Energy Reviews*, 39, 426-443. https://doi.org/10.1016/j.rser.2014.07.093

Lubis, L. A., Ghosh, D. P., & Hermana, M. (2016). Elastic and electrical properties evaluation of low resistivity pays in Malay Basin clastics reservoirs. In IOP Conference Series: Earth and Environmental Science (Vol. 38, No. 1, p. 012004). IOP Publishing.

Maurya, S. P., & Singh, N. P. (2019). Seismic modelling of CO2 fluid substitution in a sandstone reservoir: A case study from Alberta, *Canada*. *Journal of Earth System Science*, 128(8). https://doi.org/10.1007/s12040-019-1263-x

Moghanloo, R. G., Yan, X., Law, G., Roshani, S., Babb, G., & Herron, W. (2017). Challenges associated with CO2 sequestration and Hydrocarbon Recovery. *Recent Advances in Carbon Capture and Storage*. https://doi.org/10.5772/67226

Oyediran, A. T., Salim, A. M., & Almasgari, A. A.-S. (2020). Central Luconia carbonate build-ups: A review and Future Outlook. Proceedings of the Third International Conference on Separation Technology 2020 (ICoST 2020). https://doi.org/10.2991/aer.k.201229.005

Prajapati, S., Liu, C., & Ghosh, D. (2019). Rock physics templates and anisotropy. In SEG Technical Program Expanded Abstracts 2019 (pp. 358-362). Society of Exploration Geophysicists.

Raza, A., Gholami, R., Rezaee, R., Rasouli, V., & Rabiei, M. (2019). Significant aspects of carbon capture and storage – a review. *Petroleum*, 5(4), 335–340. https://doi.org/10.1016/j.petlm.2018.12.007

Raza, A., Gholami, R., Rezaee, R., Han Bing, C., Nagarajan, R., & Ali Hamid, M. (2017). Preliminary assessments of CO2 storage in carbonate formations: a case study from Malaysia. *Journal of Geophysics and Engineering*, 14(3), 533-554.

Refael, R., Hermana, M., & Hossain, T. M. (2022). Optimization of Amplitude Versus Offset Attributes for Lithology and Hydrocarbon Indicators Using Recurrent Neural Network. *Natural Resources Research*, 1-18.

Ridwan, T. K., Hermana, M., Lubis, L. A., & Riyadi, Z. A. (2020). New avo attributes and their applications for facies and hydrocarbon prediction: A case study from the northern malay basin. *Applied Sciences*, 10(21), 7786.

Subrahmanyam, D., & Rao, P. H. (2008, January). Seismic attributes-A review. In 7th international conference & exposition on petroleum geophysics, Hyderabad (pp. 398-404).

The SEG wiki. SEG Wiki. (n.d.). Retrieved February 12, 2022, from https://wiki.seg.org/wiki/Main_Page

White, R. E. (1991). Properties of instantaneous seismic attributes. *The Leading Edge*, 10(7), 26-32.

Pigott, J. D., Kang, M. H., & Han, H. C. (2013). First order seismic attributes for clastic seismic facies interpretation: Examples from the East China Sea. *Journal of Asian Earth Sciences*, 66, 34-54.

Tiwari, P. K., Das, D. P., Patil, P. A., Chidambaram, P., Low, Z., Chandran, P. K., ...& Tewari, R. D. (2021). Offshore MMV Planning for Sustainability of CO2.

Vera, V. C., & Lawton, D. C. (2010). Fluid substitution and seismic modelling in a sandstone aquifer. CREWES Res. Rep., 22, 29.

Warrlich, G. M., Adams, E. W., Ryba, A., Tam, T., Ting, K. K., & Tang, H. K. (2019). What matters for flow and recovery in carbonate gas reservoirs: Insights from the mature Central Luconia Province, offshore Sarawak, Malaysia. *AAPG Bulletin*, 103(3), 691-721.

Wei Kiat, C., Menier, D., Jamaludin, S. N., & Ghosh, D. (2016, March). Geomorphology and karstification of the Southern field high carbonates in Central Luconia Province. In Offshore Technology Conference Asia. OnePetro.